In-Flight Calibration of the ROSAT HRI UV Sensitivity

M. Barbera and G. Micela
Osservatorio Astronomico G.S. Vaiana ,Palermo, Italy

A. Collura
Istituto per le Applicazioni Interdisciplinari della Fisica (CNR), Palermo, Italy

S.S. Murray and M.V. Zombeck
Harvard-Smithsonian Center For Astrophysics, Cambridge (MA), USA

ABSTRACT

Comparing measured and estimated count rates of a few selected sample stars, we confirm the validity and provide the in-flight calibration of the ROSAT HRI UV/Visible effective area model in Zombeck et al. 1997, ApJ, 487, L69.

The count rate estimates for Betelgeuse derived with this model are in agreement with the measured HRI upper limit. This result is also confirmed in an erratum by Berghöfer et al. (2000, A&A, 357, 387) aimed at revising their previous calculation (Berghöfer et al. 1999, A&A, 342, L17) which was overestimated by more than two orders of magnitude.

Adopting this ROSAT HRI UV/Visible effective area model and measured UV/Visible spectra of a set of sample stars covering the range of T_{eff} 3000-40000 K, we have built the calibration curves to estimate UV/Visible contamination count rates for any star of known T_{eff}, m_v, and N_H.

Subject headings: instrumentation: detectors — stars: early type — stars: late type — ultraviolet: stars — X-rays: stars

1. Introduction

The unexpected UV sensitivity of the ROSAT HRI (David et al. (1995)) has been a compelling issue, both for the interpretation of the HRI data of sources with a potential UV component, and for the design and calibration of the HRC on board the Chandra X-ray Observatory (Murray et al. (1997)), a multichannel plate detector similar to the ROSAT and Einstein HRIs.

The paper by Zombeck et al. (1997) (in the following: paper I) has provided experimental evidence that the excess ROSAT HRI UV sensitivity is due to a higher than originally expected transmission of the UV/Ion blocking filters. At least two effects are responsible for this higher transmission: oxidation of the aluminum layers, and resonant interference introduced by their multilayer design (Barbera et al. (1997)). As a result a significant contribution to the HRI UV sensitivity occurs at wavelengths longer than 2000 Å in agreement with pulse height distributions observed for hot stars indicating UV detections at wavelengths longer than 1850 Å (in-flight calibration line).

The HRI UV quantum efficiency model given in Figure 4 of paper I is based on laboratory measurements of back-up filters and microchannel plates. It shows that besides the sensitivity at wavelengths longer than 2000 Å a contribution to the UV sensitivity is still present in the 1200-2000 Å band previously ascribed as the only source of UV leak in the Einstein HRI (Schmitt et al. (1985)). Given the inadequate knowledge of the UV/Visible sensitivity of CsI coated microchannel plates, the HRI effective area model presented in paper I provides two different curves for wavelengths longer than 2500 Å . These are representative of the lower and upper limits for the actual HRI UV sensitivity.

Berghöfer et al. (1999) claimed that the effective area model presented in paper I overestimates the HRI quantum efficiency at wavelengths longer than 2500 Å and support this argument on the basis of a comparison between the measured upper limit to the HRI count rate for Betelgeuse and the count rate they estimated using that model. More recently, stimulated by our further investigations on the subject, these authors have recalculated the Betelgeuse estimated HRI count rate and found a new estimate about two orders of magnitude lower and in agreement with the validity of the model in paper I (Berghöfer et al. (2000)).

In order to verify the accuracy of the UV/Visible effective area model presented in paper I and to provide an in-flight calibration of the model, we have analyzed a set of sample stars of different spectral types observed with both the ROSAT PSPC and HRI. The UV/Visible spectra of these sample stars, which have been folded with the HRI effective area model to estimate the expected UV/Visible contamination, are based on IUE observations (1200-3250 Å) of the sample stars, and normalized optical calibrated spectra of parent spectral type stars (3500-7400 Å).

Once the HRI UV/Visible effective area model, based on laboratory measurements (paper I), is validated and calibrated with the use of ROSAT HRI in-flight measurements, we can use this model to estimate the expected UV/Visible count rate contamination for stellar observations conducted with the ROSAT HRI.

In section 2 we compare the measured HRI count rates for a set of sample stars with the estimated count rates based on our effective area model provided in paper I. In section 3 we show for which spectral type stars it is important to account for possible HRI UV/Visible contamination, and provide the curves to estimate the HRI count rates due to UV/Visible contamination for any star of given photospheric effective temperature (T_{eff}), apparent visual magnitude (m_v), and interstellar hydrogen column density (N_H).

2. In-flight calibration of the HRI UV/Visible effective area model

In order to provide the in-flight calibration of the HRI UV/Visible effective area model presented in paper I, we have selected a set of sample stars observed with both the ROSAT PSPC and the HRI detectors, where an IUE calibrated low dispersion spectrum was available. Beside a few early type stars where the UV/Visible contamination can be significant, we have also included, for completeness, few late type stars.

Table 1 lists the selected sample stars including the measured ROSAT PSPC and HRI count rates. To estimate the HRI UV/Visible contamination count rates, we have used measured calibrated spectra. The UV spectra of the sample stars in the wavelength range 1200-3250 Å are based on calibrated low dispersion spectra taken with the International Ultraviolet Explorer (IUE), and available in the public archive maintained by the European Space Agency at VILSPA (http://iuearc.vilspa.esa.es/). The visible spectra 3500-7400 Å have been derived from calibrated spectra of parent spectral type stars in Jacoby et al. (1984). The gap between 3250 Å and 3500 Å has been filled with a linear interpolation between the UV and the visible spectra. Table 1 lists the ID numbers of the specific IUE observations used for each sample star. As an example, Figure 1 shows the calibrated UV/Visible spectrum of Betelgeuse.

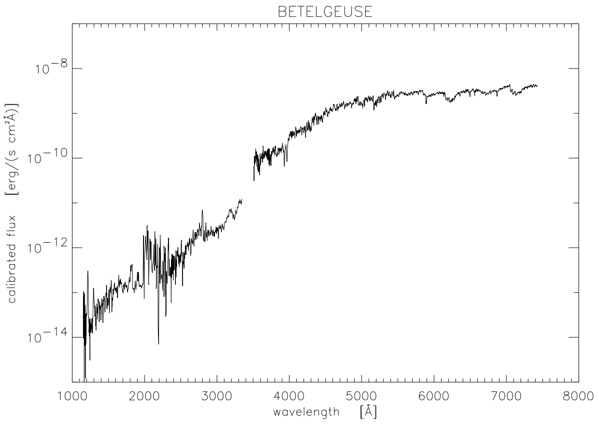

Fig. 1.— UV/Visible calibrated spectrum of Betelgeuse

Table 2 reports the estimated count rates in different wavelength ranges derived using the HRI effective area model published in paper I. The last column gives the measured ROSAT HRI UV/Visible contamination count rate. Notice that for the stars with negligible X-ray emission, inferred from the ROSAT PSPC measurement, the measured ROSAT HRI UV/Visible contamination count rate coincides with the measured HRI rate (see Table 1). For the other stars, the measured PSPC rate has been converted into the expected X-ray HRI rate using the PIMMS software with a single temperature Raymond-Smith (RS) model. This rate was then subtracted from the measured HRI rate to derive the residual UV/Visible contamination rate. The parameters used in the RS model are namely: HD46150 (KT=0.86 keV, NH = 2.2e21), ζ Ori (KT=0.22 keV, NH=3.0e20), γ Cas (KT=0.86 keV, NH = 2.0e20), Alcyone (KT=0.86 keV, NH = 2.0e20), Hz-2168 (KT=0.86 keV, NH = 2.0e20), GJ 124 (KT=0.86 keV, NH = 1.0e18), GJ 139 (KT=0.86 keV, NH = 1.0e18). The log(NH) is available in the literature for all these stars. The temperature has been taken from Berghöfer et al. (1996) for ζ Ori, and γ Cas, while for the other stars we have used a typical value of KT=0.86 keV. The uncertainty in the plasma temperature should not introduce a relative uncertainty larger than 20% in the estimated PSPC to HRI rate conversion factor.

For all our sample stars, the estimated ROSAT HRI count rates, resulting from the leak in the 1200-5500 Å band, are consistent with the measured total count rates.

The estimated count rates suggest that a non-negligible contribution to the HRI UV sensitivity comes at wavelengths longer than 2500 Å. As discussed in paper I, the poor knowledge of the microchannel plate quantum efficiency at wavelengths longer than 2500 Å results in a somewhat uncertain knowledge of the HRI effective area at these wavelengths. The two models provided in paper I above 2500 Å define the range where the actual HRI effective area should be located. The comparison between estimated and measured count rates for early type stars, and in particular the detections, suggests that the actual HRI effective area is likely to be closer to the high effective area model provided in paper I.

In the case of the late type star Betelgeuse, the UV contamination is only at wavelengths longer than 2000 Å with a non-negligible contribution in the wavelength range 4000-5500 Å. The ROSAT HRI upper limit to the count rate from Betelgeuse is consistent with both the effective area models given in paper I and therefore, we cannot put new constraints on our knowledge of the ROSAT HRI UV/Visible sensitivity. The same argument is valid for the two nearby G type stars (GJ124, GJ139) where the estimated UV/Visible contamination is very low and consistent with the measured rate.

Our estimate of the HRI count rate for Betelgeuse is only within a factor of two to three with respect to the new estimate given by Berghöfer et al. (2000). The small difference between our estimate and the one in Berghöfer et al. (2000) is likely due to the fact that they use a Kurucz synthetic spectrum for Betelgeuse, while we use a measured calibrated spectrum of a parent spectral type star.

The comparison between HRI in-flight measurements and predicted UV/Visible contamination rates, here presented for a few sample stars, confirm that the HRI UV/Visible effective area model provided in paper I is fully representative of the in-flight performance of the instrument.

In the next section we use the model provided in paper I to establish for which spectral type stars it is important to account for possible UV/Visible contamination in the ROSAT HRI observations, and to quantitatively estimate the amount of this contamination.

3. The HRI UV/Visible contamination for stellar sources

In order to provide useful calibration curves to estimate the HRI UV/Visible count rates from stars of different spectral types, we have selected a set of stars, covering the entire range of T_{eff} 3000 - 40000 K, where a low dispersion IUE calibrated spectrum was available. Notice that the choice of these stars is nearly arbitrary and is driven by the attempt to provide a good coverage of the above mentioned T_{eff} range.

Table 3 lists some relevant information about this new set of stars including the reference number of the adopted IUE low dispersion calibrated spectra.

The dereddened visible spectra (3500-7400 Å) for these stars were derived from calibrated spectra of parent spectral type stars in Jacoby et al. (1984). The IUE spectrum of each one of these stars was dereddened, according to Seaton (1979), using the appropriate hydrogen column density (see Table 3). The dereddened UV/Visible spectra of the sample stars were then normalized to $m_v = 0$, and attenuated by a given interstellar hydrogen column density N_H ranging from 1×10^{19} cm^{-2} (nearly unabsorbed) to 5×10^{21} cm^{-2}. Figure 2 shows the dereddened UV/visible spectrum of one of the sample stars (top curve) and an example of how the absorption of an interstellar hydrogen column density of 2×10^{21} cm^{-2} affects the UV/visible stellar spectra.

The UV/visible spectra of the sample stars, normalized to $m_v = 0$, have been folded with the UV/Visible HRI effective area model, provided in paper I. Figure 3 shows the curves of estimated HRI rate (1200-5500 Å) as a function of T_{eff} and hydrogen column density for stars of $m_v = 0$. At wavelengths longer than 2500 Å we have used the estimated HRI rate derived with the higher effective area model in Paper I (logarithmic interpolation). These curves can be used to estimate the UV/Visible contamination rate in the ROSAT HRI observations of any star with known m_v, T_{eff}, and N_H.

The linear regression plot of HRI count rate vs. U magnitude given in Figure 2 of Berghöfer et al. (1999) represents one single point in our plot corresponding to $T_{eff} \approx 10000$ K, and $N_H \approx 1 \times 10^{19}$ cm^{-2}. Applying their plot to other spectral type stars (e.g. a B0 star with T_{eff} about 30000 K) or to higher hydrogen column density (e.g. $N_H \geq 2 \times 10^{21}$ cm^{-2}) may introduce an error of more than a factor of ten in the estimate of the HRI UV/Visible contamination count rates. The correlations provided in Figures 1 and 2 of Berghöfer et al. (1999) are, therefore, only valid for stars in the narrow spectral type range B8-A2, and low interstellar absorption ($N_H < 10^{20}$ cm^{-2}).

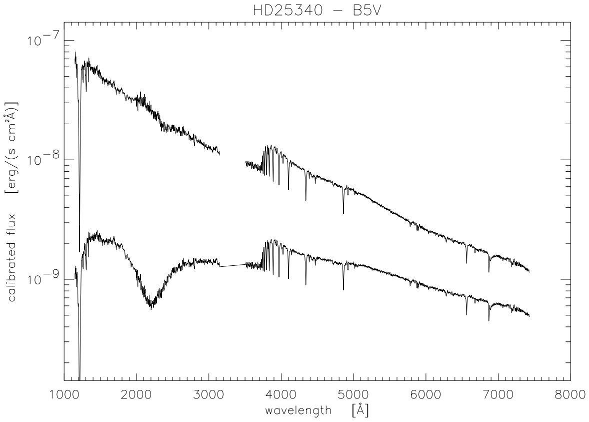

Fig. 2.— UV/Visible calibrated spectrum of the sample star HD25340 (B5V). The top curve is the dereddened spectrum while the bottom curve is the same spectrum attenuated by an interstellar hydrogen column density of 2×10^{21} cm^{-2}.

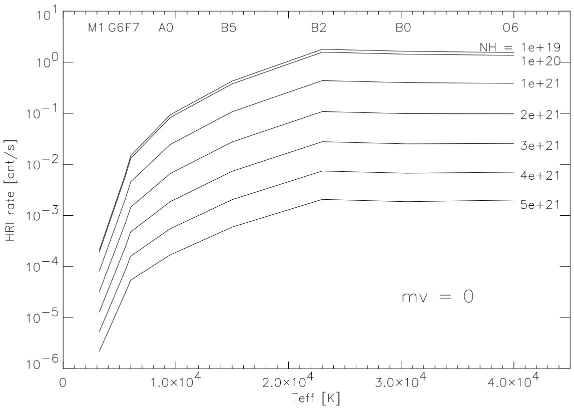

Fig. 3.— Estimated HRI rate (1200-5500 Å) for stars normalized to $m_v = 0$ as a function of T_{eff} and N_H.

Figure 4 is a plot of the ratio of UV/Visible (1200-5000 Å) to X-ray (0.1-2.4 keV) count rates for unabsorbed main sequence stars. The adopted dereddened HRI UV/Visible count rates have been previously described, while the adopted unabsorbed HRI X-ray count rates have been derived from the available ROSAT PSPC archival data of the sample stars converted into an HRI X-ray rate using the PIMMS software and a single temperature RS model with KT = 0.86 keV, and the interstellar absorption of each individual star given in Table 3.

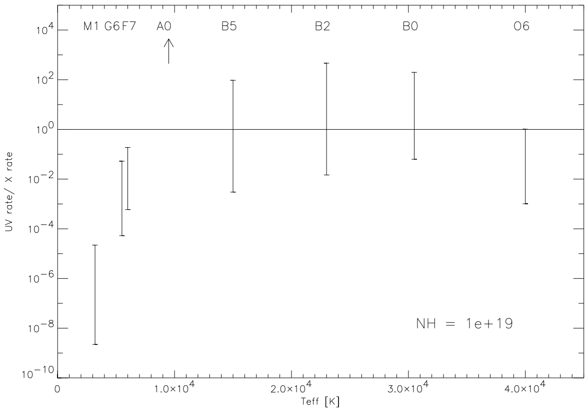

Fig. 4.— Ratio of the UV/Visible (1200-5500 Å) to X-ray (0.1-2.4 keV) HRI rate for main sequence stars as a function of T_{eff}. The bar on each data point takes into account the known range of X-ray activity for each spectral type.

For each spectral type star we have assumed a range of X-ray luminosity based on the literature and listed in Table 4.

We notice that the UV/Visible contamination for late type stars (F-M types) is always negligible. For A type stars, so far not known to be X-ray emitters, the HRI measurements can be considered entirely due to UV contamination. For early type stars the relevance of the UV contamination depends on the X-ray activity.

Figure 4 is a quick look reference plot useful to understand for which spectral type stars and which level of X-ray activity it is necessary to account for possible UV/Visible contamination in an HRI observation. However, the usage of the curves in Figure 3 is recommended for a more quantitative estimate of the specific HRI UV/Visible contamination for a given star with known m_v, N_H, and T_{eff}.

In order to estimate the HRI UV/Visible contamination from other non-standard stellar spectrum sources we suggest to fold the UV/Visible spectrum of the source with the HRI effective area model we provided in paper I and available in tabular format at the WEB page http://hea-www.harvard.edu/HRC/rosat/uvqe.txt.

4. Summary and Conclusions

The ROSAT HRI UV/Visible effective area model presented in paper I is based on laboratory measurements conducted within the ROSAT HRI ground calibration program. To provide an in-flight calibration of this model we have selected a set of stars observed with both the ROSAT PSPC and the HRI where the UV/Visible calibrated spectrum was also available.

The comparison between measured and model estimated UV/Visible contamination rates for this set of stars confirms the validity of the ground calibration model in paper I. These results also suggest that the actual HRI UV/Visible effective area is likely closer to the high sensitivity model (logarithmic interpolation) among the two provided in paper I at wavelengths longer than 2500 Å.

The count rates estimated with the two models for Betelgeuse, a late type giant with a cool photosphere and also negligible X-ray emission, are both in agreement with the measured HRI upper limit. Our estimate of the HRI count rate for Betelgeuse is only within a factor of two to three with respect to the new estimate given by Berghöfer et al. (2000) in an erratum recently published to revise their previous estimate (Berghöfer et al. (1999)) which was more than two order of magnitude higher.

Since the UV/Visible contamination on HRI observations is strongly dependent on the source spectrum and on the interstellar absorption, we have provided useful calibration curves to estimate the HRI UV/Visible contamination count rates from any star of given T_{eff}, m_v, and N_H.

The UV/Visible contamination for late type stars in the spectral type range G-M is always negligible. For the F type stars a small non-negligible UV contamination may be present in the case of very faint X-ray sources ($L_x < 10^{27}$ $ergs/s$). For A type stars, HRI count rates can be entirely attributed to UV contamination. For early type stars the degree of UV/Visible contamination depends on the X-ray activity and N_H and can be a very large fraction of the detected count rates, especially for B type stars.

We acknowledge partial support by Agenzia Spaziale Italiana (MB, AC, GM), Ministero della Ricerca Scientifica e Tecnologica (MB, AC, GM), and NASA contract NA8-38248 (MVZ, SSM). We acknowledge usage of the IUE Final Archive maintained by the European Space Agency at VILSPA, the SIMBAD astronomical database of the Centre de Donnée astronomiques de Strasbourg, and the ROSAT data archive of the Max Planck Institut für extraterrestrische Physik.

REFERENCES

Barbera, M., Collura, A., Dara, A., Leone, M., Powell, F.R., Serio, S., Varisco, S., & Zombeck, M.V. 1997, Exp. Astr., 7, 51

Berghöfer, T.W., Schmitt, J.H.M.M., & Cassinelli, J.P. 1996, A&AS, 118, 481

Berghöfer, T.W., Schmitt, J.H.M.M., Danner, R., & Cassinelli, J.P. 1997, A&A, 322, 167

Berghöfer, T.W., Schmitt, J.H.M.M., & Hünsch, M. 1999, A&A, 342, L17

Berghöfer, T.W., Schmitt, J.H.M.M., & Hünsch, M. 2000, A&A, 357, 387

Cohen, D.H., Cassinelli, J.P., & MacFarlane, J.J., 1997, ApJ, 487, 867

Damiani, F., Maggio, A., Micela, G., Sciortino, 1997, ApJ, 483, 350

David, L.P., Harden, F.R., Jr., Kearns, K.E., & Zombeck, M.V., February 1995, 'The ROSAT High Resolution Imager', U.S. ROSAT Science Data Center

Jacoby, G.H., Hunter, D.A., & Christian, C.A. 1984, ApJS, 56, 257

Micela, G., Sciortino, S., Kashyap, V., Harden, F.R., Jr., Rosner, R., 1996, ApJS, 102, 75

Micela, G., Sciortino, S., Harden, F.R., Jr., Kashyap, V., Rosner, R., Prosser, C.F., Damiani, F., Stauffer J., Caillault, J.P., 1999, A&A, 341, 751

Murray, S.S., Chappell, J.H., Kenter, A.T., Kobayashi, K., Kraft, R.P., Meehan, G.R., Zombeck, M.V., Fraser, G.W., Pearson, J.F., Lees, J.E., Brunton, A.N., Pearce, S.E., Barbera, M., Collura, A., & Serio, S. 1997, SPIE, 3114, 11

Schmitt, J.H.M.M., Golub, L., Harnden, F.R., Jr., Maxson, C.W., Rosner, R., & Vaiana, G.S. 1985, ApJ, 290, 307

Schmitt, J.H.M.M., Fleming, T.A., & Giampapa, M.S., 1995, ApJ, 450, 392

Schmitt, J.H.M.M., 1997, A&A, 318, 215

Seaton, M.J. 1979, MNRAS, 187, 73P

Zombeck, M.V., Barbera, M., Collura, A., & Murray, S.S. 1997, ApJ, 487, L69 (Paper I)

This 2-column preprint was prepared with the AAS LATEX macros v4.0.

Table 1: List of adopted sample stars with both PSPC and HRI observations

Star	HR	HD	Sp	V	PSPC rate	HRI rate	IUE Spectra
		46150	O6e	6.75	0.056 $\pm$0.002 (1)	0.018$\pm$0.001 (1)	SWP08325, LWR07268
ζ Ori	1948	37742	O9Iab	1.70	1.45 $\pm$0.01 (1)	0.700$\pm$0.005 (1)	SWP33048, LWP11671
γ Cas	264	5394	B0IVe	2.39	3.79 $\pm$0.03 (1)	1.336$\pm$0.008 (1)	SWP33893, LWP13607
Alcyone	1165	23630	B7III	2.87	$<$ 0.003 (2)	0.0138$\pm$0.0008 (3)	SWP08020, LWR07078
Hz-2168	1178	23850	B8III	3.62	$<$ 0.006 (2)	0.0072$\pm$0.0015 (3)	SWP11245, LWR09867
Rigel	1713	34085	B8Iab	0.12	$<$ 0.0015 (4)	0.1960$\pm$0.0096 (4)	SWP31880, LWP11654
Vega	7001	172167	A0V	0.03	$<$ 0.001 (4)	0.0937$\pm$0.0035 (4)	SWP27024, LWP07904
β Aur	2088	40183	A2IV	1.85	$<$ 0.002 (4)	0.0078$\pm$0.0019 (4)	SWP50172, LWP27602
β Car	3685	80007	A2IV	1.70	$<$ 0.0004 (4)	0.0111$\pm$0.0010 (4)	SWP43459, LWP22059
GJ 124	937	19373	G0V	4.05	0.055 $\pm$0.002 (5)	0.011$\pm$0.002 (1)	SWP02663, LWR02376
GJ 139	1008	20794	G8V	4.27	0.0070$\pm$0.0005 (5)	0.0029$\pm$0.0009 (1)	SWP14039, LWR12242
Betelgeuse	2061	39801	M1	0.50	$<$ 0.012 (4)	$<$ 0.0005 (4)	SWP37517, LWP19982

[1]archival data processed by SASS

[2]Micela et al. (1996)

[3]Micela et al. (1999)

[4]Berghöfer et al. (1999)

[5]archival data processed by the Wavelet detection algorithm in Damiani et al. (1997)

Table 2: Estimated and measured HRI UV/Visible contamination count rates.

Star	Estimated Rates (1)					Measured Rate
	1200-2000 [Å]	2000-2500 [Å]	2500-4000 [Å]	4000-5500 [Å]	1200-5500 [Å]	
HD46150	$2\ 10^{-4}$	$2\ 10^{-4}$	$2\ 10^{-5}$	$3\ 10^{-8}$	$3\ 10^{-4}$	$< 5\ 10^{-3}$ (2)
			$2\ 10^{-4}$	$2\ 10^{-6}$	$5\ 10^{-4}$	
ζ Ori	$4\ 10^{-2}$	$7\ 10^{-2}$	$9\ 10^{-3}$	$5\ 10^{-6}$	$1\ 10^{-1}$	$3\ 10^{-1}$ (2)
			$6\ 10^{-2}$	$3\ 10^{-4}$	$2\ 10^{-1}$	
γ Cas	$3\ 10^{-2}$	$4\ 10^{-2}$	$4\ 10^{-3}$	$3\ 10^{-6}$	$7\ 10^{-2}$	$< 3\ 10^{-1}$ (2)
			$3\ 10^{-2}$	$2\ 10^{-4}$	$9\ 10^{-2}$	
Alcyone	$3\ 10^{-3}$	$5\ 10^{-3}$	$6\ 10^{-4}$	$1\ 10^{-6}$	$9\ 10^{-3}$	0.014 ± 0.002 (2)
			$5\ 10^{-3}$	$8\ 10^{-5}$	$1\ 10^{-2}$	
Hz-2168	$2\ 10^{-3}$	$2\ 10^{-3}$	$3\ 10^{-4}$	$7\ 10^{-7}$	$4\ 10^{-3}$	0.007 ± 0.002 (2)
			$2\ 10^{-3}$	$4\ 10^{-5}$	$6\ 10^{-3}$	
Rigel	$3\ 10^{-2}$	$6\ 10^{-2}$	$7\ 10^{-3}$	$2\ 10^{-5}$	$9\ 10^{-2}$	0.1960 ± 0.0096
			$7\ 10^{-2}$	$9\ 10^{-4}$	$2\ 10^{-1}$	
Vega	$2\ 10^{-2}$	$3\ 10^{-2}$	$4\ 10^{-3}$	$2\ 10^{-5}$	$6\ 10^{-2}$	0.0937 ± 0.0035
			$4\ 10^{-2}$	$1\ 10^{-3}$	$9\ 10^{-2}$	
β Aur	$2\ 10^{-3}$	$3\ 10^{-3}$	$5\ 10^{-4}$	$3\ 10^{-6}$	$6\ 10^{-3}$	0.0078 ± 0.0019
			$5\ 10^{-3}$	$2\ 10^{-4}$	$1\ 10^{-2}$	
β Car	$3\ 10^{-3}$	$5\ 10^{-3}$	$6\ 10^{-4}$	$4\ 10^{-6}$	$8\ 10^{-3}$	0.0111 ± 0.0010
			$6\ 10^{-3}$	$2\ 10^{-4}$	$1\ 10^{-2}$	
GJ 124	$1\ 10^{-7}$	$3\ 10^{-5}$	$3\ 10^{-6}$	$3\ 10^{-7}$	$3\ 10^{-5}$	$< 1\ 10^{-3}$ (2)
			$6\ 10^{-5}$	$1\ 10^{-5}$	$1\ 10^{-4}$	
GJ 139	$6\ 10^{-8}$	$7\ 10^{-6}$	$1\ 10^{-6}$	$2\ 10^{-7}$	$8\ 10^{-6}$	$< 1\ 10^{-3}$ (2)
			$6\ 10^{-5}$	$6\ 10^{-6}$	$7\ 10^{-5}$	
Betelgeuse	$4\ 10^{-7}$	$5\ 10^{-6}$	$1\ 10^{-6}$	$3\ 10^{-6}$	$1\ 10^{-5}$	< 0.0005
			$7\ 10^{-5}$	$6\ 10^{-5}$	$1\ 10^{-4}$	

[1] The two values quoted for the estimated count rate at wavelengths longer than 2500 Å are derived with the two HRI different effective area models in paper I.

[2] The measured PSPC rate has been converted into the expected X-ray HRI rate using the PIMMS software and adopting a single temperature Raymond-Smith (RS) model. This rate has been subtracted from the measured HRI rate to derive the UV/Visible contamination rate. The adopted parameters for the RS model are namely: HD46150 (KT=0.86 keV, NH = 2.2e21), ζ Ori (KT=0.22 keV, NH=3.0e20), γ Cas (KT=0.86 keV, NH = 2.0e20), Alcyone (KT=0.86 keV, NH = 2.0e20), Hz-2168 (KT=0.86 keV, NH = 2.0e20), GJ 124 (KT=0.86 keV, NH = 1.0e18), GJ 139 (KT=0.86 keV, NH = 1.0e18).

Table 3: List of sample stars covering the T_{eff} range 3000-40000 K.

Star	HR	HD	Sp	V [mag]	T_{eff} [K]	$\log(N_H)$ [cm^{-2}]	IUE Spectra
	8023	199579	O6V	5.96	40000	21.04	SWP09429, LWP03855
υ ORI	1855	36512	B0V	4.62	30000	20.35	SWP08164, LWR07097
λ LIB	5902	142096	B2.5V	5.03	20000	21.09	SWP42326, LWR10778
35 ERI	1244	25340	B5V	5.28	15000	20.06	SWP49909, LWP27312
Vega	7001	172167	A0V	0.03	9500	18.00	SWP27024, LWP07904
70 TAU	1391	27991	F7V	6.46	6500	19.00	SWP09853, LWR06639
V911 TAU		28099	G6V	8.12	5500	19.00	SWP09873, LWP02601
Betelgeuse	2061	39801	M1I	0.50	3200	19.80	SWP37517, LWP19982

Table 4: Adopted 0.1-2.4 keV X-ray luminosity range for main sequence stars.

Sp	T_{eff} [K]	log (L_x) erg/s	Reference
O6V	40000	31.0 - 34.0	1
B0V	30000	29.0 - 32.5	1,2
B2.5V	20000	27.5 - 32.0	1,2
B5V	15000	27.5 - 32.0	1,2
A0V	9500	< 25.5	3
F7V	6500	27.0 - 29.5	3
G6V	5500	26.5 - 29.5	3
M2V	3200	25.5 - 29.5	4

REFERENCES. - (1) Berghöfer et al. (1997); (2) Cohen, D.H. et al. (1997); (3) Schmitt (1997); (4) Schmitt et al. (1995).